

# Numerical Simulation of Transonic Buffet over a Supercritical Airfoil

Sébastien Deck\*

ONERA, 92322 Châtillon Cedex, France

A zonal detached eddy simulation (DES) method is presented that predicts the buffet phenomenon on a supercritical airfoil at conditions very near shock buffet onset. Some issues concerning grid generation, as well as the use of DES for thin-layer separation, are discussed. The periodic motion of the shock is well reproduced by averaged Navier–Stokes equations (URANS) and zonal DES, but the URANS calculation has needed to increase the angle of attack compared to the experimental value and the standard DES failed to reproduce the self-sustained motion in the present calculation. The main features, including spectral analysis, compare favorably with experimental measurements (Jacquin, L., Molton, P., Deck, S., Maury, B., and Soulevant, D., “An Experimental Study of Shock Oscillation over a Transonic Supercritical Profile,” AIAA Paper 2005-4902, June 2005). A very simple model based on propagation velocities yields the main frequency of the motion. As suggested by Lee (Lee, B. H. K., “Transonic Buffet on a Supercritical Airfoil,” *Aeronautical Journal*, May 1990, pp. 143–152), this calculation highlights that upstream propagating waves are generated by the impingement of large-scale structures on the upper surface of the airfoil in the vicinity of the trailing edge. These upstream propagating waves can regenerate an instability leading to a feedback mechanism.

## Introduction

THE transonic buffet is an aerodynamic phenomenon that results in a large-scale self-sustained motion of the shock over the surface of the airfoil. The onset of this phenomenon is not related to any fluid/structure interaction, although it is inevitable that some structural deformation may be present. Indeed, the unsteady behavior of the flow may lead to structure vibrations termed buffeting that can lead to fatigue failure. Design standards for aircraft limit the intensity of the buffeting phenomenon because the large variation of lift associated with buffet limits the cruising speed of aircraft. The assessment of buffet onset associated with the proper computation of unsteady viscous flow around airfoil remains an outstanding problem in aerodynamics. In this study, we only focus on aerodynamic buffet on a two-dimensional rigid airfoil that is characterized by a periodic motion of the shock over the airfoil.

The periodic motion associated with this phenomenon is much larger than the timescales of the wall-bounded turbulence. Hence, there has been considerable interest in numerical approaches solving averaged Navier–Stokes equations (URANS). Past research<sup>1–3</sup> has revealed that the accuracy of the numerical calculations is mainly dictated by the accuracy of the turbulence model. Almost all of the simulations are concerned with two-dimensional calculations. A complete study (turbulence models, numerical schemes) of URANS calculations concerning the OAT15A supercritical airfoil has been recently performed by Brunet.<sup>4</sup> His study shows that URANS calculations are able to predict quite well the main properties of the flow (rms, pressure distribution) but often need to increase the angle of attack in the calculation compared to the experimental value.

At conditions very near shock buffet onset, the numerical simulation of transonic buffet is a very challenging and difficult case for detached eddy simulation (DES). More precisely, DES has been developed to handle massive separated flows that rapidly develop strong instabilities associated with large-scale structures, which overwhelms the turbulence inherited from upstream boundary

layers. This is not the case in the present work exhibiting thin-layer separation. Nevertheless, not very many publications<sup>5</sup> are devoted to DES of thin-layer separation, especially when shock/boundary-layer interactions occur.<sup>6</sup>

The objective of the current study is twofold: 1) to assess the capability of DES to capture the buffet phenomenon at the experimental angle of attack and 2) to analyze unsteady features of the flow to discuss the mechanisms of buffet onset.

## Numerical Method

### General Description

The solver FLU3M code has been developed by ONERA. It solves the Navier–Stokes equations on multiblock structured grids. The computational domain is divided by blocks; each block is composed of structured hexahedral cells. The Navier–Stokes equations are discretized using a second-order accurate upwind finite volume scheme and a cell-centered discretization. The Euler fluxes are discretized by a modified AUSM + (P) upwind scheme, which is fully described in Ref. 7.

Unsteady (global time-step) and three-dimensional Navier–Stokes simulations are highly CPU demanding. Explicit schemes are not efficient enough for this purpose, and implicit schemes are required. Time discretization is based on second-order accurate Gear’s formulation and was introduced by Pécier.<sup>8</sup> Moreover, the implicit formulation results in inversion of a large sparse matrix system. The lower–upper (LU) factorization simplifies the inversion of the latter implicit system. Further details concerning the numerical method and implementation of turbulence models can be found in Refs. 9 and 10.

This numerical method is the same as the one already used to perform large eddy simulation (LES) of the flow around a two-dimensional wing profile in near-stall conditions,<sup>7</sup> as well as around a low-pressure turbine blade,<sup>11</sup> and has also been successfully used to compute LES of the flow over a cavity at high Reynolds number.<sup>12</sup>

### DES

Hybrid approaches using a combination of Reynolds-averaged Navier–Stokes (RANS) approaches and LES have become increasingly important in the past few years. (For example, see Refs. 13–16.) Both approaches have their own advantages and drawbacks. RANS tends to be able to predict attached flows very well with a low computational cost. On the other hand, LES has a high computational cost but can predict separated flows more accurately.

Received 7 April 2004; revision received 8 December 2004; accepted for publication 22 January 2005. Copyright © 2005 by Sébastien Deck. Published by the American Institute of Aeronautics and Astronautics, Inc., with permission. Copies of this paper may be made for personal or internal use, on condition that the copier pay the \$10.00 per-copy fee to the Copyright Clearance Center, Inc., 222 Rosewood Drive, Danvers, MA 01923; include the code 0001-1452/05 \$10.00 in correspondence with the CCC.

\*Research Scientist, Applied Aerodynamics Department, 29 Avenue de la Division Leclerc.

The hybrid approach that has probably drawn most attention is the DES, which was proposed by Spalart et al.<sup>17</sup> This method has given encouraging results for a wide range of flow configurations exhibiting massive separations.<sup>18–21</sup> Here again, the motivation for this approach was to combine the best features of the RANS approach with the best features of LES. Therefore, the DES treatment of turbulence is aimed at the prediction of separated flows at unlimited Reynolds numbers and at a reasonable cost. This hybrid RANS/LES method can produce good results for separated flows in which unsteadiness is strongly self-sustaining, for example, massive separations. One of the objectives of this study is to assess the capability of a zonal DES method to capture numerically a self-sustained motion exhibiting thin-layer separation and to compare this method with standard DES results. In the following, a brief description of the standard DES model is first given before the motivations to give zonal features to this model are explained.

The DES model was originally based on the Spalart–Allmaras RANS model, which solves a one-equation turbulence model for the eddy viscosity  $\tilde{\nu}$ :

$$\frac{D\rho\tilde{\nu}}{Dt} = c_{b1}\tilde{S}\rho\tilde{\nu} + \frac{1}{\sigma}[\nabla \cdot (\mu + \rho\tilde{\nu})\nabla\tilde{\nu} + c_{b2}\rho(\nabla\tilde{\nu})^2] - \rho c_{w1}f_w\left(\frac{\tilde{\nu}}{d}\right)^2 \quad (1)$$

The eddy viscosity is defined as

$$\mu_t = \rho\tilde{\nu}f_{v1} = \rho\nu_t \quad (2)$$

To ensure that  $\tilde{\nu}$  equals  $\kappa y u_\tau$  in the log layer, in the buffer layer and viscous sublayer a damping function  $f_{v1}$  is defined as

$$f_{v1} = \chi^3 / (\chi^3 + c_{v1}^3), \quad \chi = \tilde{\nu}/\nu \quad (3)$$

The vorticity magnitude  $S$  is modified such that  $\tilde{S}$  maintains its log-layer behavior ( $\tilde{S} = u_\tau/\kappa y$ ):

$$\tilde{S} = \sqrt{2\Omega_{ij}\Omega_{ij}f_{v3}} + \frac{\tilde{\nu}}{\kappa^2 d^2}f_{v2}, \quad \Omega_{ij} = \frac{1}{2}\left(\frac{\partial\tilde{u}_i}{\partial x_j} - \frac{\partial\tilde{u}_j}{\partial x_i}\right) \quad (4)$$

which is accomplished with help of the functions

$$f_{v2} = 1 - \chi/(1 + \chi f_{v1}), \quad f_{v3} = 1 \quad (5)$$

To obtain a faster decaying behavior of destruction in the outer region of the boundary layer, a function  $f_w$  is used:

$$f_w(g) = g\left(\frac{1 + c_{w3}^6}{g^6 + c_{w3}^6}\right)^{\frac{1}{6}}, \quad g = r + c_{w2}(r^6 - r) \\ r = \frac{\tilde{\nu}}{\tilde{S}\kappa^2 d^2} \quad (6)$$

where  $g$  acts as a limiter that prevents large values of  $f_w$ . Both  $r$  and  $f_w$  are equal to one in the log layer and decrease in the outer region. Constants of the model are

$$c_{b1} = 0.1355, \quad c_{b2} = 0.622, \quad \sigma = \frac{2}{3}, \quad \kappa = 0.41 \\ c_{w1} = (c_{b1}/\kappa^2) + [(1 + c_{b2})/\sigma], \quad c_{w2} = 0.3, \quad c_{w3} = 2 \\ c_{v1} = 7.1 \quad (7)$$

For the current research, the transition terms were turned off, and we refer to the original papers<sup>22,23</sup> for further details on the constants and the quantities involved.

What is important here is that the model is provided with a destruction term for the eddy viscosity that contains  $d$ , the distance to the closest wall. This term, when balanced with the production term, adjusts the eddy viscosity to scale with local deformation rate  $\tilde{S}$ , producing an eddy viscosity given by

$$\tilde{\nu} \sim \tilde{S}d^2 \quad (8)$$

Following these arguments, Spalart et al. suggested replacing  $d$  with a new length  $\tilde{d}$  given by

$$\tilde{d} = \min(d, C_{DES}\Delta) \quad (9)$$

where  $\Delta = \max(\Delta_x, \Delta_y, \Delta_z)$  is the computational mesh size. The use of the maximum grid extension is physically justified because it controls which wavelengths can be resolved and the eddy viscosity level. More precisely, in the attached boundary layer, due to the significant grid anisotropy ( $\Delta_x \approx \Delta_z \gg \Delta_y$ ) typical of this flow region, in accordance with Eq. (9),  $\tilde{d} = d$ , and the model reduces to the standard Spalart–Allmaras (SA) RANS model. Otherwise, once a field point is far enough from the walls ( $d > C_{DES}\Delta$ ), the length scale of the model performs as a subgrid-scale version of the SA model.

However, standard DES introduces a significant dependency into the RANS part of the simulation that requires a near-wall grid spacing in the tangential direction that is larger than the boundary-layer thickness at this location. This grid resolution requirement may be easily violated in industrial simulations. In practice, switching to the LES mode may occur inside the RANS boundary layer leading to a “grid-induced-separation”<sup>15</sup> at arbitrary locations on the body. The region corresponding to  $d \approx \Delta$  is called the “gray-zone” of DES<sup>17,24</sup> because it is not clear what exactly happens in this region. Nikitin et al.<sup>25</sup> used DES as a wall-layer model in calculations of plane channel flow with different grids. The skin-friction coefficient was underpredicted by approximately 15% in most cases. The same underprediction aspect has also been observed by Caruelle<sup>2</sup> in the case of a DES calculation of a flat plate on a LES grid. More recently, Piomelli et al.<sup>26</sup> studied more closely this intermediate blending region within the DES approach. They performed LES of the flow in a plane channel at high Reynolds number by varying the location and extent of this blending layer. Their study shows that the DES buffer layer is characterized by very long eddies with unphysically long timescales. Improvements were obtained by reducing the value of  $C_{DES}$  to bring the outerflow eddies closer to the wall.

To avoid this problem in the attached boundary layer, we develop in the present study a zonal DES, in which attached boundary-layer regions are explicitly treated in RANS mode regardless of the grid resolution. This means that following the example of RANS/LES coupling, the user has to define the RANS and LES zones. In addition, the gray zone is locally forced to treat the entire shock/boundary-layer interaction in RANS mode.<sup>27</sup> This means that the DES limiter is overridden and maintains full RANS behavior to predict boundary-layer separation. This explicit character of the splitting of the flow zones differs from other RANS/LES coupling because no turbulent fluctuations are reconstructed at the interface<sup>28–31</sup> between RANS and LES in the present work.

The computational grid has to then be carefully designed. For example, in the LES region (outside boundary layers), the grid is designed to obtain nearly cubic grid cells to use the cube root  $\Delta = (\Delta_x\Delta_y\Delta_z)^{1/3}$  as a filter width for LES. This simple modification decreases drastically the level of predicted eddy viscosity because the latter is proportional to the square of the filter width  $\Delta$ . We also made the choice to remove the near-wall functions in LES mode formulation. (See also Ref. 32.) Thus,

$$f_{v1} = 1, \quad f_{v2} = 0, \quad f_w = 1 \quad (10)$$

These modifications will theoretically modify the value of the additional model constant  $C_{DES} = 0.65$  that was calibrated by Shur et al.<sup>33</sup> using isotropic turbulence with the original near wall functions. However the resulting slight modification of  $C_{DES}$  should not be crucial (as discussed in a private communication with P. R. Spalart in 2002), and the present study was performed with the original value 0.65. Furthermore, if one postulates a local equilibrium between production and destruction, the already mentioned relation  $\tilde{\nu} \sim \tilde{S}d^2$  becomes

$$\langle \nu_t \rangle = \underbrace{C_{DES}^2 (c_{b1}/c_{w1})}_{0.1332} \Delta^2 \langle S \rangle \quad (11)$$

which is similar to the well-known Smagorinsky model but with a smaller constant because  $C_{Smag} = 0.18$  and because of a change in

the definition of  $S$ . Some authors<sup>34–36</sup> highlight that the comparison with Smagorinsky’s model cannot be performed completely because we do not know exactly if the grid size  $\Delta$  is really the cutoff scale. It is only known to be of the order of  $\Delta$ . Breuer et al.<sup>32</sup> compared DES and LES for the separated flow around a flat plate at high incidence when the same grid resolution was applied. They studied the influence of a few parameters and, in particular, the effect of changing definition of  $S$  [ $S = \sqrt{(2\Omega_{ij}\Omega_{ij})}$  for DES and  $S = \sqrt{(2S_{ij}S_{ij})}$  for LES] and showed that this difference is not responsible for observed discrepancies between LES and DES.

Our approach is called zonal DES, which is in a slight contradiction with the core of the DES idea because DES produces a single hybrid model, the switch to LES mode being governed by the grid. However, note that DES is well adapted to treat massively separated flows, for example, the separation being most often fixed by the geometry, which is not the case in the present work exhibiting thin-layer separation.

### OAT15A Supercritical Airfoil

This study is focused on the supercritical OAT15A airfoil. Experiments were carried out in the S3Ch continuous research wind tunnel of ONERA’s Chalais Meudon center. The test section is square, and the dimensions of the test chamber are  $0.78 \times 0.78 \text{ m}^2$ . A detailed description of the experimental arrangement, equipment, and results is given by Molton and Jacquin<sup>37</sup> and Jacquin et al.<sup>38</sup>

The OAT15A airfoil has a chord equal to  $c = 230 \text{ mm}$ , a thickness-to-chord ratio  $e/c = 12.5\%$ , and a thick trailing edge of  $0.5\%$  of the chord length. Experimental transition was fixed near the leading edge at  $x/c = 7\%$  on both sides of the airfoil with a carborundum technique. Various angles of attack from  $2.5$  to  $3.91$  deg were investigated. The buffet phenomenon appeared at an angle of attack equal to  $3.25$  deg, and the main frequency of the phenomenon was about  $70 \text{ Hz}$  whatever the angle of attack. Laser Doppler velocimetry (LDV) measurements were performed for an angle of attack of  $3.5$  deg. The Reynolds number, based on the freestream velocity and the chord, is equal to  $3 \times 10^6$ , whereas the freestream Mach number is set to  $0.73$ .

### Results

#### Grids

Following the example of LES, the grid generation constitutes an important issue in DES because the grid extension controls which wavelengths can be resolved, as well as the eddy viscosity level.

To evaluate the accuracy of the different simulations, two two-dimensional grids have been evaluated first thanks to steady RANS computations because the DES grids are obtained by duplication

of these planar grids in the spanwise direction. Both basic two-dimensional grids are of C–H type in the  $(x, y)$  plane (Fig. 1). The fine grid (grid A) has been obtained from a grid convergence study on transonic buffet performed by Brunet,<sup>1</sup> and the very fine grid (grid B) has been retained from a grid convergence study issued from a drag extraction study.<sup>39</sup> Each grid is divided into two blocks. The first domain concerning the upper and lower sides of the airfoil contains  $317 \times 121$  (respectively,  $385 \times 161$  for grid B) nodes, whereas the H-type domain contains  $93 \times 289$  (respectively,  $129 \times 369$  for grid B) nodes. The far-field conditions are imposed at  $80$  times the chord length away from the profile. The first mesh point  $y^+$  always stays below one for both grids, leading, respectively, to a total number of grid points in the  $(x, y)$  plane equal to  $65,000$  for grid A and to  $110,000$  for grid B.

The pressure coefficient distribution obtained for both grids with the SA model at an angle of attack equal to  $2.5$  deg, is compared to the experiment in Fig. 2. At this angle of attack, a thin separated area exists at the foot of the shock, but no large-scale self-sustaining motion is observed experimentally. Note the very flat and characteristic pressure distribution in the supersonic zone for the supercritical OAT15A airfoil. Moreover, pressure levels are well predicted on the lower side of the airfoil as well as in the supersonic and the trailing-edge regions. Nevertheless, the computed shock location is found

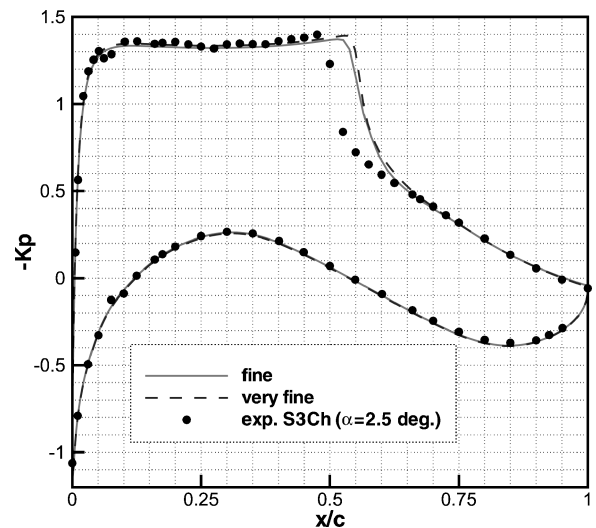


Fig. 2 Pressure coefficient around OAT15A airfoil ( $M=0.73$  and  $\alpha=2.5$  deg).

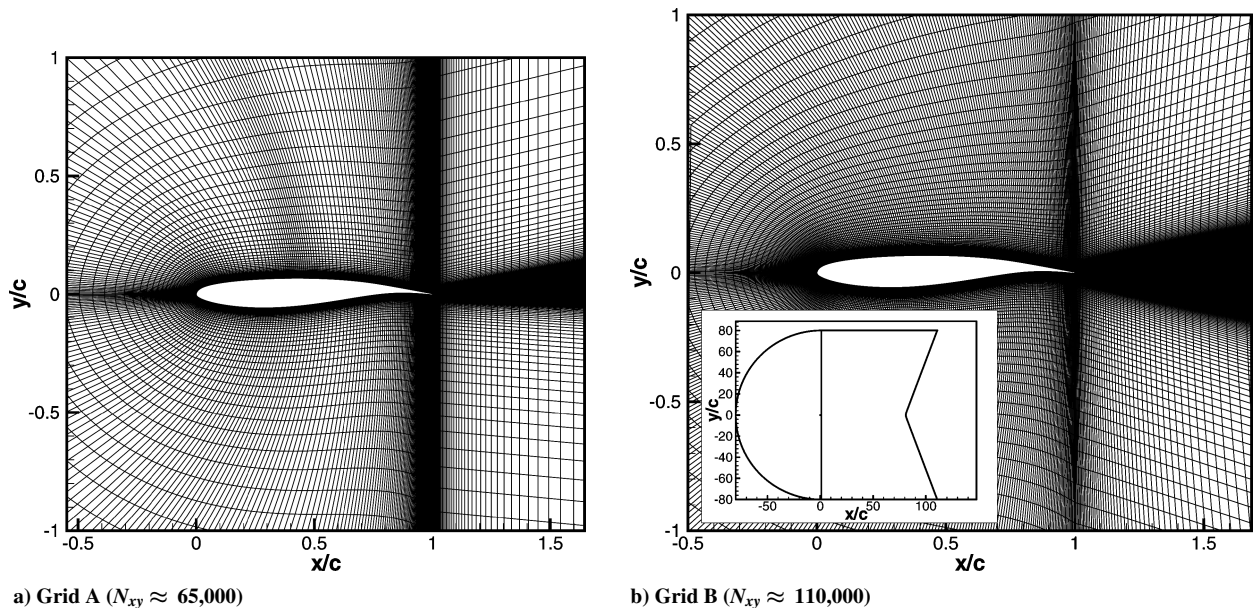


Fig. 1 Mesh around OAT15A airfoil.

farther downstream of the experimental one for both grids. It has been verified<sup>4</sup> that this downstream location of separation does not come from the treatment of transition on the upper side of the airfoil. The differences between the results yielded from the two grids are very small, and grid convergence is achieved.

The design of a DES grid around a two-dimensional airfoil requires the specification of two main grid parameters. The first one is the grid extension  $\Delta_z$  in the spanwise direction, and the second one concerns the global span size of the computational domain  $L_z = N_z \times \Delta_z$ , where  $N_z$  is the number of planes in the spanwise direction. To evaluate the effect of grid refinement, two three-dimensional grids have been built by duplicating the two-dimensional grids A and B in the spanwise direction. The three-dimensional grids are not named for the sake of simplicity.

In the present work, the grid extension  $\Delta_z$  is chosen constant, for example, uniformly distributed in the homogeneous direction, to have  $\Delta_x \approx \Delta_z$  in the LES region, following Spalart's recommendations.<sup>34</sup> The standard DES formulation needs to choose the grid extension  $\Delta_z$  in the spanwise and tangential directions, larger than the boundary-layer thickness  $\delta$  at that location, to avoid grid-induced separation. This methodology has been used for grid A, for example,  $(\Delta z)_{\text{gridA}} \geq \delta$ . Grid B has a higher resolution in both the streamwise and tangential directions, and the switching to LES mode according to Eq. (9) occurs inside the boundary layer. To avoid grid-induced separation, the full RANS behavior is maintained in domain 3 (Fig. 3) as long as  $(\Delta y)_{\text{gridB}} < (\Delta z)_{\text{gridA}}$ . That means that the switching into LES mode is forced in grid B and corresponds to the natural switching to LES mode for grid A. Hence, this grid design strategy allows one to compare the effect of grid refinement in the LES regions with a same RANS region. In addition, the zonal-DES simulation is performed only in domains 3 and 6, enabling a RANS solution on the lower side of the airfoil.

The second important issue is the choice of the grid spanwise width. In the case of a backward facing step<sup>40</sup> of height  $H$ , a spanwise domain width of 4 to 6 $H$  is considered to be a minimum to be able to capture the three-dimensional mechanisms at low frequencies. If one assumes that at low angles of attack the maximum thickness of the separated region in the  $(x, y)$  plane is equal to the half-thickness of the airfoil  $e/2$ , the width of the spanwise domain has to conform to

$$L_z/c \geq 4e/2c = 0.246 \quad (12)$$

The spanwise grid can then be obtained by simple duplication of the basic grid. Therefore, the mesh size can become prohibitive

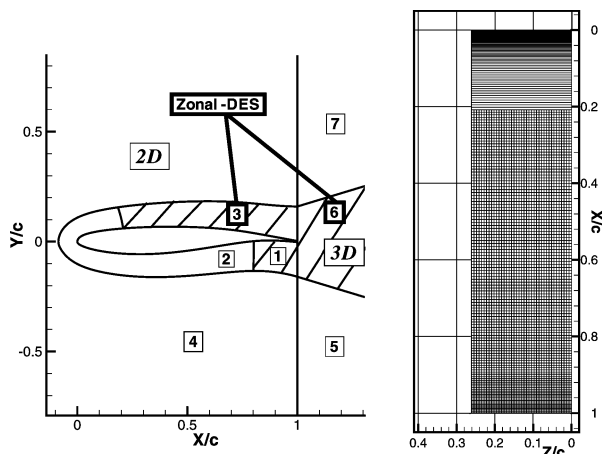


Fig. 3 Two-three-dimensional grid.

because this dense resolution must be kept in the far field and in the wake with a structured solver. In the framework of the LESFOIL project, Mary and Sagaut<sup>7</sup> (see also Ref. 11) developed a two-/three-dimensional coupling method to optimize the cell distribution. The main idea is related to the specificity of external flows around an infinite span body, which consists of the existence of a large zone where the flow is two dimensional. Indeed, three-dimensional computations can be limited to a zone close to the airfoil where the flow is turbulent, whereas two-dimensional simulations are performed in the far field (except in the wake). This strategy does not affect the accuracy of the simulation as long as the two-/three-dimensional interface is located in regions where the flow is two dimensional. Hence, the grid used for the present DES computation is presented Fig. 3, which illustrates the two- and three-dimensional domains in the  $(x, y)$  plane as well as the solid boundary mesh on the upper side of the airfoil  $[(x, z)$  plane].

The main characteristics of the different three-dimensional grids are summarized in Table 1.

Grid A is called three-dimensional because it has been obtained by simple duplication of the basic grid in the  $(x, y)$  plane in the spanwise direction. Grid B contains an overall number of seven domains and is called two-/three-dimensional because only three domains require a three-dimensional simulation (Fig. 3). This grid strategy allows division of the total number of grid points by a factor of two ( $2 \times 10^6$  grid points instead of  $4 \times 10^6$  with a classical three-dimensional meshing strategy). It has been verified in a previous study<sup>41</sup> of the global three-dimensional grid that the flowfield is effectively two dimensional on the lower side of the airfoil. The normalized spanwise width of the grid is equal to 26% (respectively, 40% for grid A) of the chord following assumption (12). Also note that grid B has a grid resolution in the spanwise direction that is twice as high as that of grid A for the same number of grid points.

### Computation Description

The comparison of the capabilities of URANS, standard DES, and zonal-DES approaches to predict the buffet phenomenon is of interest.

In the present work, a URANS calculation is performed with the SA model. At the experimental value of angle of attack, that is,  $\alpha = 3.5$  deg, all unsteady calculations with the SA model lead inevitably to a steady solution whatever the grid and numerical parameters used. A higher angle of attack of  $\alpha = 4.5$  deg was needed to obtain the self-sustained unsteady phenomenon according to Ref. 4. Furthermore, the present standard DES calculation failed<sup>41</sup> to predict the shock motion at  $\alpha = 3.5$  deg, and a higher angle of attack ( $\alpha = 4$  deg) was needed to obtain an unsteady solution. Conversely, zonal-DES computations are performed at the experimental angle of attack ( $\alpha = 3.5$  deg) and the self-sustained motion is obtained. These numerical results will be discussed more precisely in the following section.

Standard and zonal-DES computations are carried out in three steps. First, a URANS calculation provides an initial flow solution. After the transient phase, the real unsteady calculations begin.

The simulations are carried out on a single processor of an NEC-SX6 supercomputer and the code is running approximately at 4 giga floating point operations. The time step is fixed at  $\Delta t_{\text{cid}} = 0.5 \mu\text{s}$ , for example,  $\Delta t = 0.5 \times 10^{-6} (U_\infty/c) = 5 \times 10^{-4}$  with four Newton inner iterations yielding a Courant–Friedrichs–Lewy number based on acoustic velocity and spanwise grid spacing less than one. The CPU cost per cell and per inner iteration is 1  $\mu\text{s}$ .

### Flowfield Description

Figure 4 (issued from the zonal-DES calculation) illustrates the main characteristics of the flow. The turbulent structures are

Table 1 Grid size characteristics

| Grid | Method    | Two-/three-dimensional | 100 $L_z/c$ | $N_z$ | 100 $\Delta z/c$ | 100 $C_{\text{DES}} \Delta z/c$ | $N_{xy}$ | $N_{xyz}$               |
|------|-----------|------------------------|-------------|-------|------------------|---------------------------------|----------|-------------------------|
| A    | DES       | No                     | 40          | 31    | 1,3              | 1.04                            | 65,000   | $\approx 2 \times 10^6$ |
| B    | Zonal DES | Yes                    | 26          | 41    | 0,65             | 0.42                            | 110,000  | $\approx 2 \times 10^6$ |

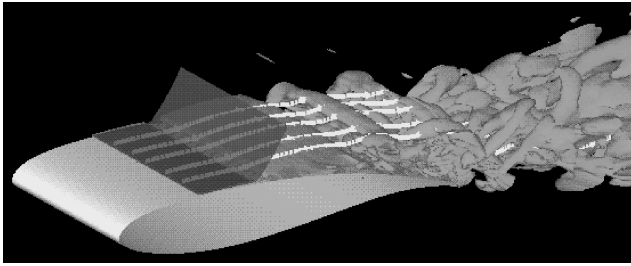


Fig. 4 One isocontour of  $Q$  criterion and sonic surface ( $\alpha = 3.5$  deg).

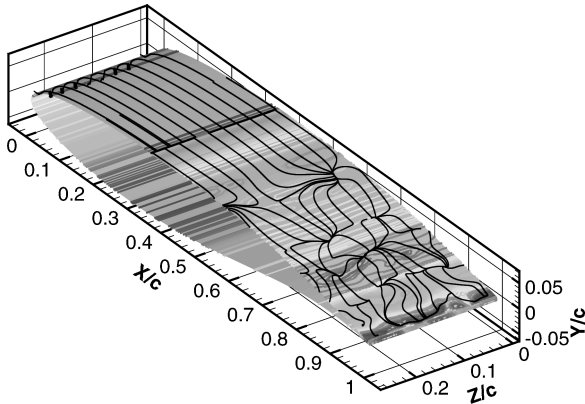


Fig. 5 Instantaneous wall pressure distribution and skin-friction lines ( $\alpha = 3.5$  deg, zonal DES calculation).

exhibited showing a positive value of the  $Q$  criterion,<sup>42</sup>  $Q = \frac{1}{2}(\|\Omega^2\| - \|S^2\|)$ . Figure 4 illustrates the rollup of two-dimensional eddies in the free shear layer, which progressively become three-dimensional when they impact the thick trailing edge. This impact creates smaller structures that are reentrained in the recirculating flow, leading to the three-dimensional character of the wall pressure distribution as shown in Fig. 5. This three-dimensional character of the recirculating flow is also highlighted by the skin-friction lines pattern: The different separation and reattachment lines are evidenced in Fig. 5 by the accumulation of skin-friction lines. The shock/boundary-layer interaction is treated in RANS mode, and the flow remains two dimensional in the vicinity of this interaction. In other words, the shear layer has no initial LES content, for example, unsteady three-dimensional eddies of the size of the boundary layer. As a consequence, note that the instability occurring within the shear layer in the vicinity of the trailing edge is a mechanism strong enough to permit the development of unsteady eddies. In addition, the boundary layer that develops from the trailing edge to the separation shock is treated in URANS because this boundary layer is directly affected by the three-dimensional unsteady pressure field in the recirculating zone.

**Mean and RMS Fields**

The averaging procedure is performed both in time and in the homogeneous spanwise direction during the calculation.<sup>7</sup> Averaged pressure coefficient distribution for both calculations are compared with experimental data in Fig. 6. The shock motion is also highlighted by the spreading aspect of the shock pressure distribution. This aspect is well reproduced by zonal DES and URANS at a higher angle of attack. Nevertheless, the wall pressure is a bit overestimated on the upper side with the zonal-DES calculation and is associated with a pressure level that is too low at the thick trailing edge and with an advanced location of separation. This comes from a more important separated zone on the upper side compared to the URANS calculation. Note that the motion of the shock is not obtained by standard DES ( $\alpha = 4$  deg) and URANS at experimental conditions ( $\alpha = 3.5$  deg).

Figure 7 shows the computed standard deviation of wall pressure as a function of the location on the upper side of the airfoil. One can distinguish three zones. The first one, located upstream of sep-

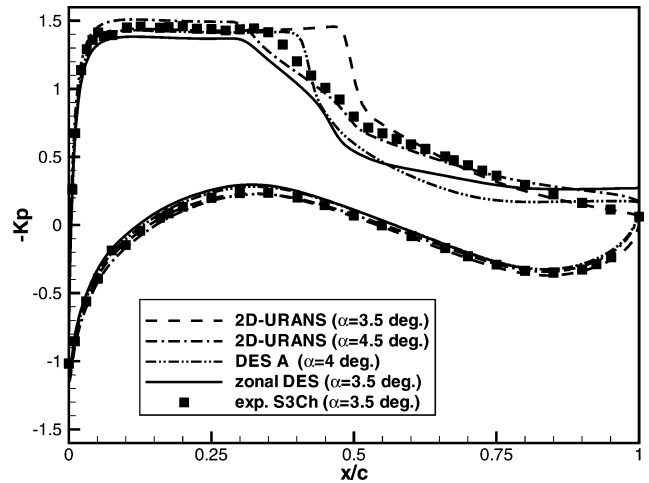


Fig. 6 Averaged pressure coefficient distribution.

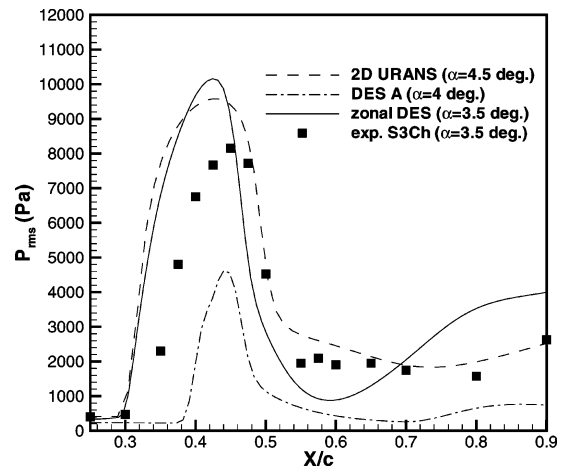


Fig. 7 Streamwise evolution of rms value.

aration ( $x/c \leq 0.3$ ), is associated with a very low level of pressure fluctuation. Then there is a rapid increase of the rms value. Finally, the last zones originate from the region located downstream of this peak and present a plateau. Wall pressure fluctuations are induced by the separated flow unsteadiness. The peak is related to the fluctuations of the separation shock, for example, the pressure fluctuates between the pressure of the attached flow and the pressure behind the separation shock. In the present calculations, the grid is not fine enough to obtain the lambda shape of the upper-side shock that is observed experimentally.<sup>37,38</sup> The computed shock is too straight, leading to a more important pressure jump and rms levels in the calculations.<sup>43</sup> However, the comparison between the computations and experiment shows a fairly good agreement except for the standard DES calculation.

Figure 8 compares computational and experimental mean streamwise velocity profiles between  $x/c = 0.28$  and  $0.75$  for URANS, DES, and zonal-DES calculations. Note the experimental thin boundary layer at location  $x/c = 0.28$  compared to calculations. Experimentally, the transition was fixed at location  $x/c = 0.07$ , whereas calculations are fully turbulent. At location  $x/c = 0.35$ , one can notice some discrepancies between the experiment and the zonal-DES calculation because the calculation leads to separation too early (Fig. 6). At location  $x/c = 0.55$ , a thin recirculation is observed experimentally, whereas the mean flow remains attached for the zonal-DES calculation. Location  $x/c = 0.75$  corresponds to the last streamwise station along the airfoil, for which LDV measurements were acquired. The thickness of the shear layer at that location obtained by the zonal-DES calculation compares favorably with experimental data.

The displacement of the shock is also highlighted in Fig. 9, showing the comparison of the rms field of longitudinal velocity

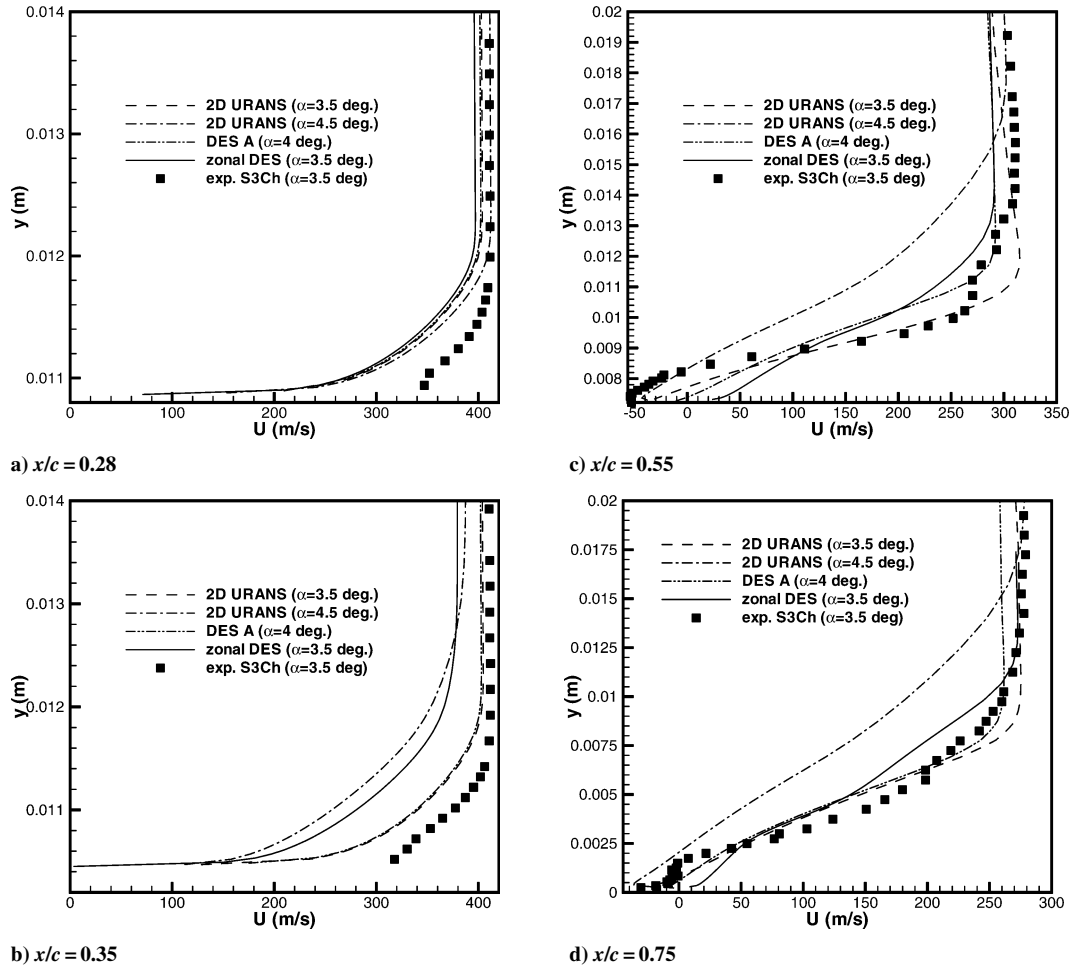


Fig. 8 Longitudinal velocity profiles.

fluctuations between calculation and LDV measurements.<sup>37,38</sup> The domain of excursion of the shock is clearly evidenced by the spreading aspect of the rms field. The URANS calculation at an angle of attack of 4.5 deg leads naturally to a higher amplitude of displacement of the shock compared to the experiment. The self-sustained shock motion is not reproduced here by standard DES, and very low levels of velocity fluctuations are obtained in the shear layer. Conversely, the amplitude of the shock displacement is well reproduced by zonal DES, even if its mean location is found too early compared to the experiment according to Fig. 6.

The rms streamwise velocity profiles are then plotted in Fig. 10. For clarity, results for the URANS calculation at  $\alpha = 3.5$  deg are not shown because the unsteady calculation leads to a steady solution. At location  $x/c = 0.28$ , the flow remains attached, and the rms value is close to zero because the boundary layer is treated in the RANS mode of DES. The nonzero computed values come from the unsteadiness of the mean field. Figure 10 also illustrates the difference between zonal DES and RANS/LES coupling because the present calculations do not use any means of seeding fluctuations within the boundary layer. At location  $x/c = 0.35$ , note that calculations lead to a level of fluctuations that is too important, which is due to a separation that is too early. Downstream of the separation point, the maximum rms value rapidly increases. The maximum of velocity fluctuations is mainly related to the normal velocity jump across the shock. This maximum value obtained by the zonal-DES calculation shows a fairly good agreement, whereas standard DES leads to levels of fluctuations in the shear layer that are too low.

#### Power Spectral Analysis

The power spectral density (PSD) function, termed  $G(f)$ , describes how the mean squared value of the wall pressure is distributed in frequency.<sup>44</sup> Note the antinomic aspect between the needs of statistics and the constraints imposed by computational fluid dy-

namics (CFD). Indeed, to perform a statistical analysis in good conditions, the signal has to be well sampled on a sufficient duration because the spectral information has to be averaged on many blocks to be statistically significant.<sup>45</sup> In practice, unsteady signals issued from CFD are most often oversampled on a short duration due to high CPU cost.<sup>46</sup> Concerning data issued from the unsteady calculation, we used a parametric autoregressive (AR) method in which the quality of the spectral estimate is quite good, even for short data records.<sup>47</sup> The AR parameters are obtained with the Burg method<sup>48</sup> (or maximum entropy method). The ability of this method to generate spectrum estimators with accurately resolved peaks (for both the frequency resolution and the energy level) while smoothing the base noise level allows more flexibility than the classical Welch's periodogram.<sup>49</sup> This method is particularly well adapted to study short data that are known to consist of sinusoids in white noise. (See Refs. 43 and 50 for examples of the use of this method in the field of fluid mechanics.)

Figure 11 compares the numerical sound pressure level (in decibels) of pressure fluctuation at several locations from  $x/c = 0.4$  to  $= 0.9$  to the corresponding experimental ones. Strong harmonic peaks are present in these spectra, clearly illustrating the periodic nature of the flow. The peak around 70 Hz is the main frequency of the buffet phenomenon, for example, the frequency of the oscillating shock motion. This important feature, illustrating the unsteadiness of the mean field, is well reproduced by zonal DES at experimental conditions ( $\alpha = 3.5$  deg) and URANS at a higher angle of attack ( $\alpha = 4.5$  deg). In the intermittent region ( $x/c = 0.4$ ), the spectra are dominated by high-amplitude and low-frequency fluctuations. One can also notice the enrichment of the spectra with regard to higher frequencies at locations farther downstream, for example, in the vicinity of the trailing edge.

More precisely, in the vicinity of the trailing edge, the experimental spectrum presents a rather flat aspect at high frequencies,

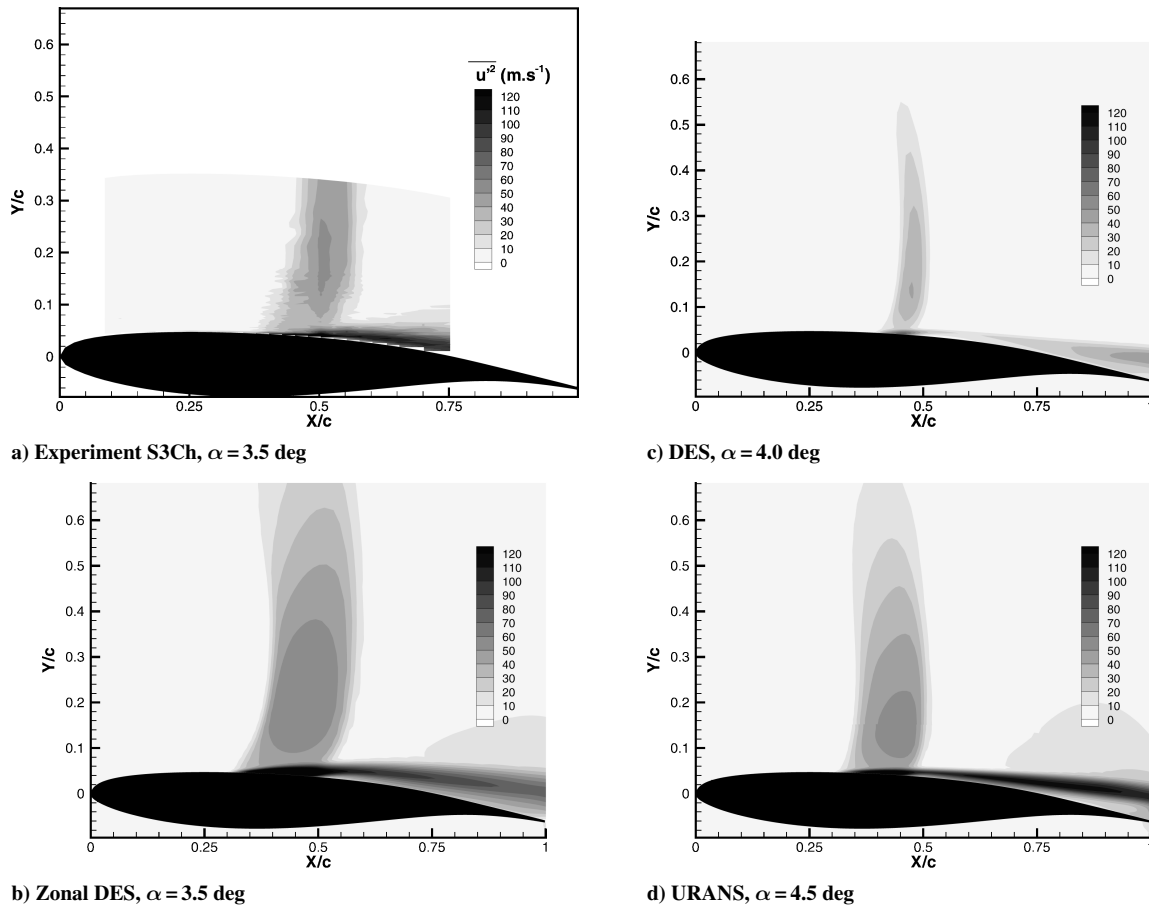


Fig. 9 Longitudinal velocity fluctuation, rms field.

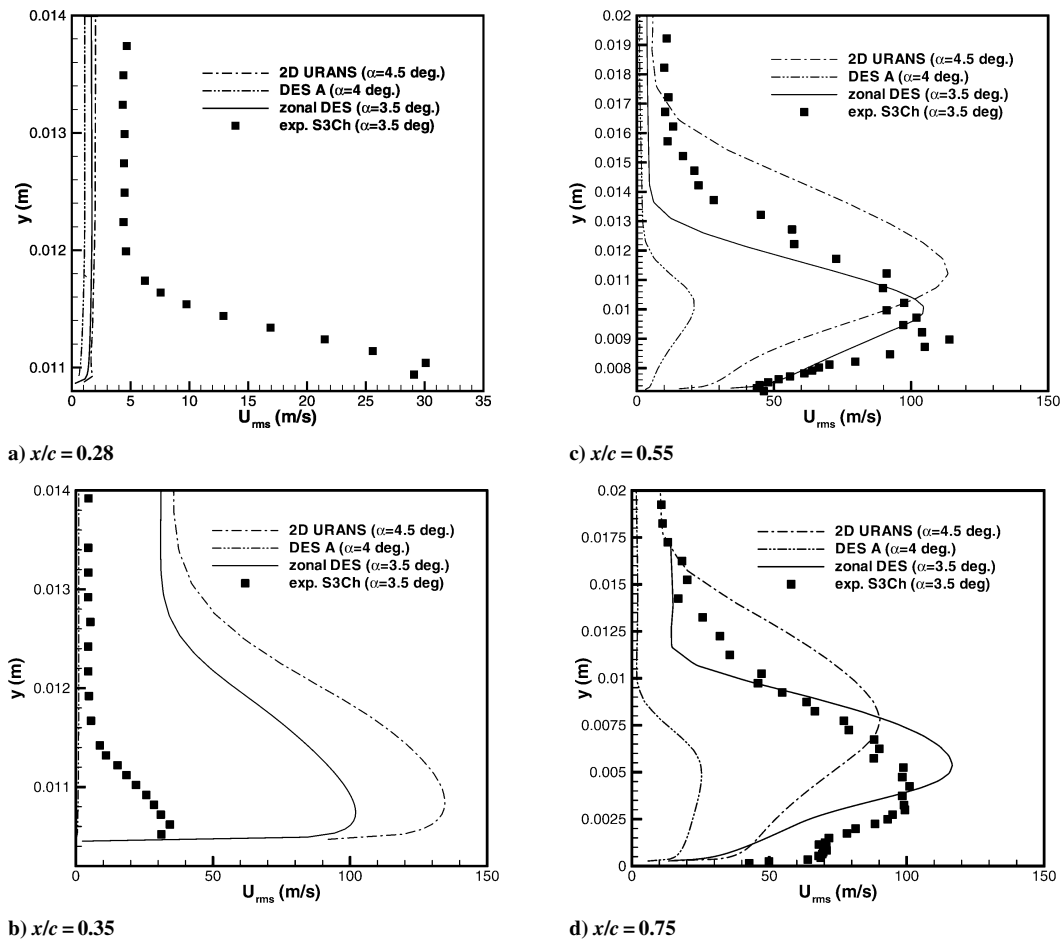


Fig. 10 Longitudinal velocity fluctuation profiles.

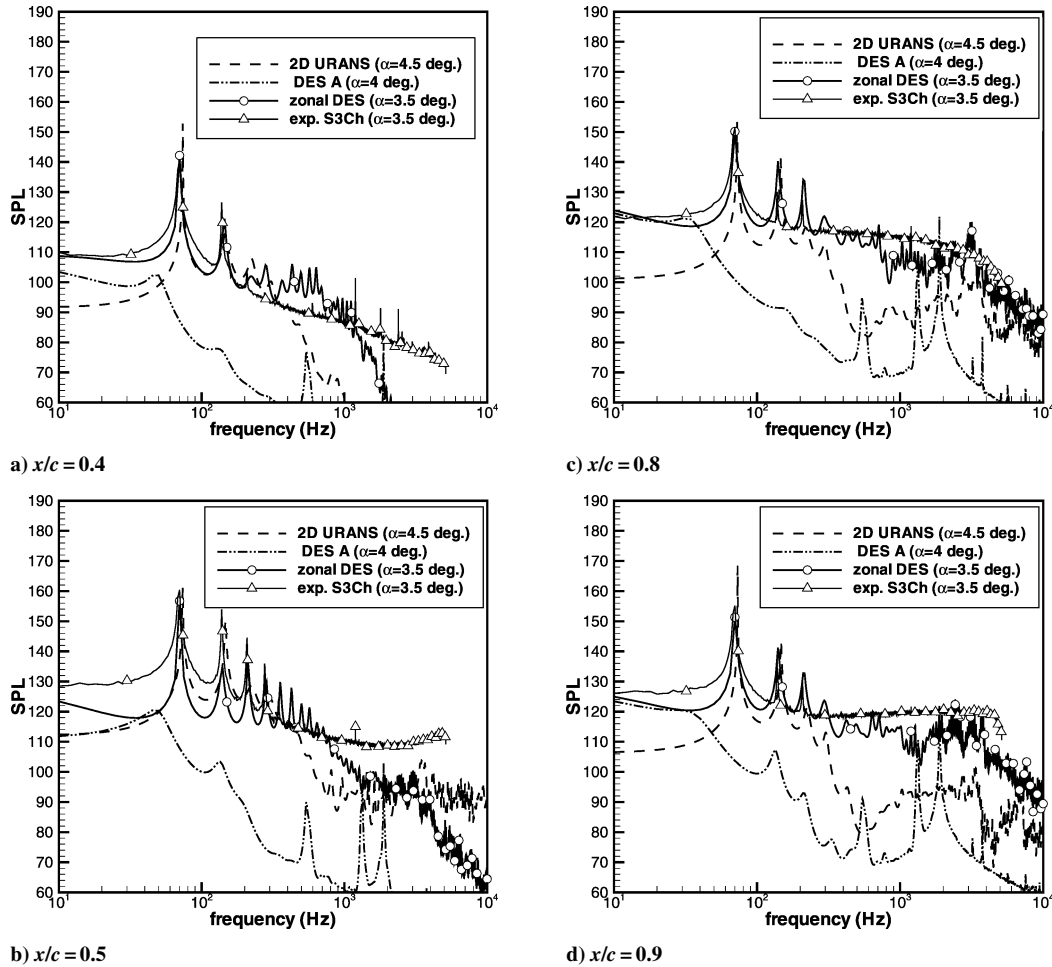


Fig. 11 PSD of pressure fluctuations.

for example, a random white noise aspect. This feature is well reproduced by zonal DES. Of course, the URANS approach is not able to predict the wideband spectrum of turbulence. In physical space, this white noise aspect corresponds to turbulent structures of different scales. The calculation suggests that these structures come partly from the rollup eddies of the free shear layer, which progressively becomes three dimensional when impacting the thick trailing edge (Fig. 4).

**Discussion of Shock Buffet Onset**

The preceding results can now be discussed in connection with possible important mechanisms in the onset of shock buffet. In this section, only the zonal-DES calculation will be considered.

Indeed, Fig. 4 has highlighted that an instability emanates from the separation point, grows along the shear layer, and interacts with the sharp trailing edge of the airfoil. It is now established<sup>51</sup> that when a shear layer interacts with a sharp edge, it produces a pressure wave that propagates upstream. This assumption can be verified in Fig. 12, which presents the instantaneous divergence field of velocity and highlights the occurrence of pressure waves. The presence of upstream waves originating at the trailing edge is clearly evidenced. More precisely, note that the impact of the large-scale structures in the vicinity of the thick trailing edge causes acoustic radiation, which in turn propagates upstream. Therefore, these upstream propagating waves can regenerate an instability leading to a feedback mechanism.<sup>52</sup> This idea has been suggested by Lee.<sup>53</sup>

More precisely, due to the motion of the shock, pressure waves are formed and propagate downstream at a velocity  $v_d$ . When reaching the trailing edge, the disturbances generate upstream-moving waves at velocity  $v_u$ . That means that the period of the shock oscillation should agree with the time  $T_d$  it takes for a disturbance to propagate

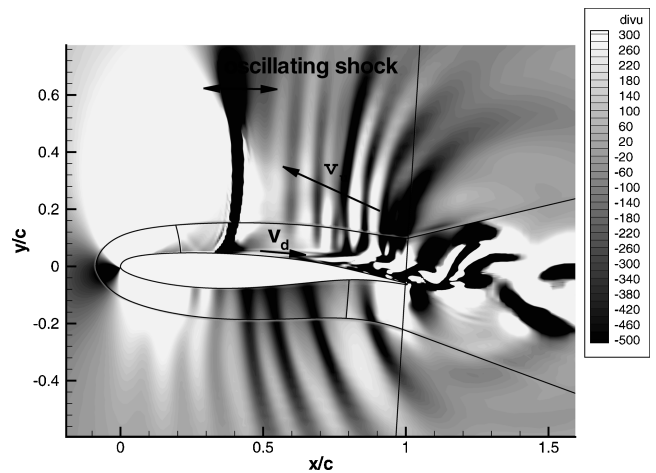


Fig. 12 Instantaneous divergence field of velocity.

from the shock to the trailing edge added to the time  $T_u$  needed for an upstream moving wave to reach the shock from the trailing edge. The total duration it takes to complete such a loop can be given by the following relation:

$$T = T_d + T_u = (c - x_s)/v_d + (c - x_s)/|v_u| \tag{13}$$

where  $c$  is the chord and  $x_s$  is the mean location of the shock wave.

This location can be obtained with a statistical analysis by plotting the streamwise evolution of the skewness of pressure fluctuations ( $S_P = \overline{P'^3} / \overline{P'^2}^{3/2}$ ). Experimental and computed streamwise

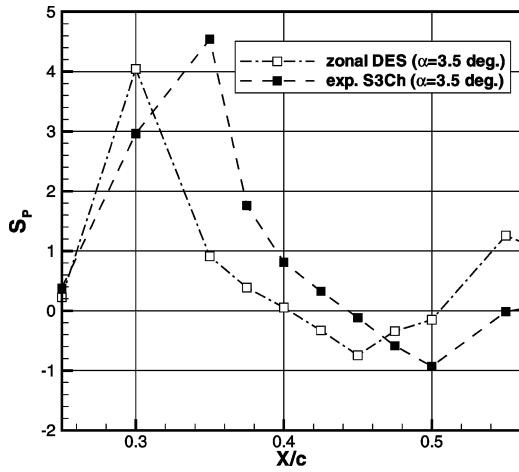
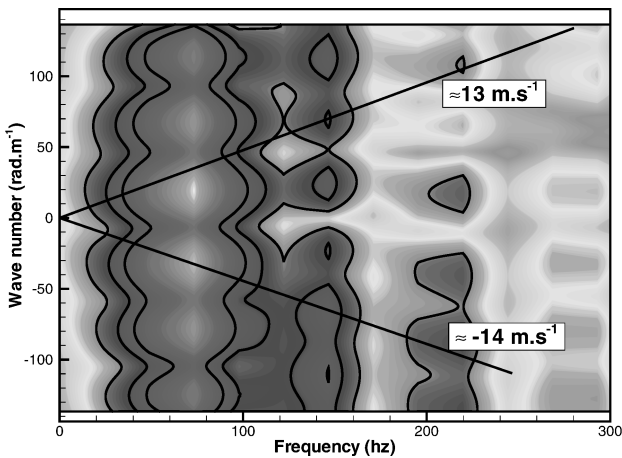
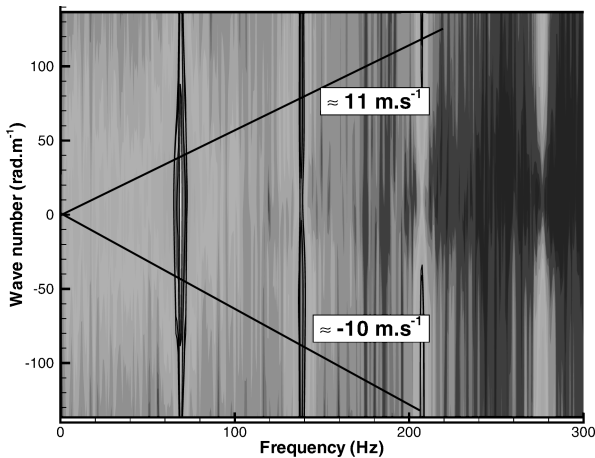


Fig. 13 Streamwise evolution of skewness factor.



a) Zonal DES calculation



b) ONERA S3Ch experiment

Fig. 14 Frequency wave number pressure spectrum.

evolution of skewness in the vicinity of the shock are shown in Fig. 13.

Note a rapid decrease of the skewness factor between locations  $x/c \approx 0.3$  and  $0.47$ , where it reaches its minimal value. The negative value can be attributed by the displacement of the shock. For example, pressure signals are dominated by negative peaks due to the intermittent presence of the shock. The high value at  $x/c \approx 0.3$  comes from the large-amplitude fluctuations caused by the passage of the shock at this location. One can assume<sup>54</sup> that its mean position corresponds to the first abscissa where  $S_p = 0$ , as shown in Fig. 13.

The velocity of upstream-traveling acoustic waves is  $v_u$ , that is,  $v_u = a(M - 1)$ , where  $a$  is the local speed of the sound and is determined thanks to the zonal-DES calculation in the field outside the separated flow region, for example,  $a = 320$  m/s and  $M = 0.86$ .

The velocity  $v_d$  of downstream-propagating waves can be obtained from the phase relation as suggested by Lee<sup>53</sup> or by using a frequency-wave number spectrum.<sup>50</sup> The result is shown in Fig. 14 for both numerical and experimental data. Two mean propagation speeds are identified: one forward at a velocity of nearly 13 m/s and one backward with an identical absolute value. The upstream velocity corresponds to the pressure waves traveling downstream at velocity  $v_d$ . Applying Eq. (13) to numerical results gives the period  $T \approx 0.0137$  s, for example, the frequency  $f = 73$  Hz. The same calculation based on experimental data leads to  $T \approx 0.0143$  s, that is, a frequency of the shock motion equal to  $f = 69$  Hz. The correlation between the calculated frequency and the frequency issued from spectral analysis is excellent considering the inaccuracies in determining upstream wave propagation velocity.

This result supports Lee's<sup>53</sup> idea of assuming that the period of shock oscillation is comparable with the time it takes for a disturbance to propagate from the shock to the trailing edge plus the time for an upstream-traveling wave generated at the trailing edge to reach the shock. In addition, the calculation highlights that the upstream-propagating waves are generated by the impingement of large-scale structures on the upper surface of the airfoil. This kind of feedback<sup>55</sup> is typical of flows with self-sustained oscillations such as flows over cavities.

### Conclusions

The numerical simulation of a transonic buffet is a problem of outstanding importance, but it is a very challenging and difficult case for DES because it presents thin-layer separation. This study has shown interest in a zonal-DES method to predict the buffet phenomenon on a supercritical airfoil. Some modifications concerning the formulation of DES have been used because the near-wall functions in LES mode have been removed, and we use the cube root  $\Delta = (\Delta_x \Delta_y \Delta_z)^{1/3}$  as a filter width for LES.

A grid topology based on a local mesh-refinement methodology has been suggested to calculate a transonic buffet over a two-dimensional airfoil. To avoid grid-induced separation on the upper side or any undesirable effects due to an unresolved attached boundary layer in the LES mode, the shock/boundary-layer interaction is explicitly treated in RANS mode, as is the lower surface of the airfoil. This method allows one to compare the effect of grid refinement in the LES regions with the same RANS boundary-layer solution.

Note that calculations have shown that large-scale structures are formed in the shear layer in the vicinity of the trailing edge and that this mechanism is strong enough to permit the development of unsteady eddies.

The periodic motion of the shock is well reproduced by URANS and zonal DES, but it is important to stress that the URANS calculation required an increase in the angle of attack compared to the experimental value. The self-sustained motion has not been recovered with standard DES, even at a higher angle of attack, in the present calculations. Conversely, the buffet phenomenon has been reproduced at the experimental value of the angle of attack with zonal DES. However, the wall pressure is a bit overestimated on the upper side with this latter calculation and is associated with a pressure level that is too low at the thick trailing edge and an advanced location of separation. This comes from a more important separated zone on the upper side. The upper-surface shock is also too straight, leading to a more important pressure jump and rms levels in the calculations because the grid is not fine enough to reproduce the lambda shape of the shock. The spectral properties of wall pressure fluctuations issued from zonal DES compare favorably with the experiment, especially the enrichment of the spectra with regard to higher frequencies at locations farther downstream, for example, in the vicinity of the trailing edge.

From a physical point of view, an instability emanates from the separation point, grows along the shear layer, and interacts with the sharp trailing edge of the airfoil. To highlight the aeroacoustical

aspect of a transonic buffet, a very simple model based on propagation velocities recovers the main frequency of the motion. This result supports Lee's idea of assuming that the period of shock oscillation is comparable with the time it takes for a disturbance to propagate from the shock to the trailing edge plus the time for an upstream-traveling wave generated at the trailing edge to reach the shock. In addition, the calculation highlights that the upstream-propagating waves are generated by the impingement of large-scale structures on the upper surface of the airfoil.

### Acknowledgments

The author gratefully acknowledges the Service Programme de l'Aéronautique from the French Ministry of Defense and Direction Générale de l'Aviation Civile from the French Ministry of transport, which granted the research reported in this paper. The author is also greatly indebted to L. Jacquin and P. Molton for supplying the experimental data, as well as to his colleagues V. Brunet and S. Esquieu for fruitful discussions on airfoil aerodynamics and to L. Larchevêque for some aspects of signal processing. E. Garnier and P. Guillen, who encouraged the author to publish, are warmly acknowledged, as is P. Duveau for his comments on the manuscript.

### References

- <sup>1</sup>Furlano, F., "Comportement des Modèles de Turbulence pour les Écoulements Découllés en Entrée de Tremblement," Ph.D. Dissertation, Dept. of Fluid Mechanics, Ecole Nationale Supérieure de l'Aéronautique et de l'Espace, Toulouse, France, March 2001.
- <sup>2</sup>Caruelle, B., "Simulations d'Écoulements Instationnaires Turbulents en Aérodynamique: Application à la Prédiction du Phénomène de Tremblement," Ph.D. Dissertation, Dept. of Fluid Mechanics, Inst. National Polytechnique de Toulouse, Toulouse, France, Oct. 2000.
- <sup>3</sup>Bartels, R. E., "Computation of Shock Buffet Onset for Conventional and Supercritical Airfoil," AIAA Paper 97-0833, Jan. 1997.
- <sup>4</sup>Brunet, V., "Computational Study of Buffet Phenomenon," AIAA Paper 2003-3679, June 2003.
- <sup>5</sup>Kotapati-Apparao, R. B., Squires, K. D., and Forsythe, J. R., "Prediction of the Flow over an Airfoil at Maximum Lift," AIAA Paper 2004-0259, Jan. 2004.
- <sup>6</sup>Fan, T. C., Xiao, J. R., Edwards, J. R., and Baurle, R. A., "Hybrid LES/RANS Simulation of a Shock Wave/Boundary Layer Interaction," AIAA Paper 2002-0431, Jan. 2002.
- <sup>7</sup>Mary, I., and Sagaut, P., "Large Eddy Simulation of Flow Around an Airfoil Near Stall," *AIAA Journal*, Vol. 40, No. 6, 2002, pp. 1139–1145.
- <sup>8</sup>Péquier, M., "Prévisions Numériques de l'Effet Magnus pour des Configurations de Munition," Ph.D. Dissertation, Dept. of Mechanical Engineering, Univ. de Poitiers, Poitiers, France, Sept. 1999.
- <sup>9</sup>Péquier, M., Guillen, P., and Caysac, R., "Magnus Effect over Finned Projectiles," *Journal of Spacecraft and Rockets*, Vol. 38, No. 4, 2001, pp. 542–549.
- <sup>10</sup>Deck, S., Duveau, P., d'Espiney, P., and Guillen, P., "Development and Application of Spalart Allmaras One Equation Turbulence Model to Three-Dimensional Supersonic Complex Configurations," *Aerospace Science and Technology*, Vol. 6, No. 3, 2002, pp. 171–183.
- <sup>11</sup>Raverdy, B., Mary, I., Sagaut, P., and Liamis, N., "High-Resolution Large-Eddy Simulation of the Flow Around a Low Pressure Turbine Blade," *AIAA Journal*, Vol. 41, No. 3, 2003, pp. 390–397.
- <sup>12</sup>Larchevêque, L., Labbé, O., Mary, I., and Sagaut, P., "LES of a Compressible Flow past a Deep Cavity," *Physics of Fluids*, Vol. 15, No. 1, 2003, pp. 193–210.
- <sup>13</sup>Speziale, C. G., "Turbulence Modeling for Time-Dependent RANS and VLES: A Review," *AIAA Journal*, Vol. 36, No. 2, 1998, pp. 173–184.
- <sup>14</sup>Batten, P., Goldberg, U., and Chakravarthy, S., "LNS—An Approach Towards Embedded LES," AIAA Paper 2002-0427, Jan. 2002.
- <sup>15</sup>Menter, F. R., Kuntz, M., and Bender, R., "A Scale-Adaptive Simulation Model for Turbulent Flow Predictions," AIAA Paper 2003-0767, 2003.
- <sup>16</sup>Kok, J. C., Dol, H. S., Oskam, H., and van der Ven, H., "Extra-Large Eddy Simulation of Massively Separated Flows," AIAA Paper 2004-0264, Jan. 2004.
- <sup>17</sup>Spalart, P., Jou, W. H., Strelets, M., and Allmaras, S. R., "Comments on the Feasibility of LES for Wings and on a Hybrid RANS/LES Approach," *Proceedings of the 1st AFSOR International Conference on DNS/LES*, edited by C. Liu and Z. Liu, Greyden, Columbus, OH, 1998, pp. 137–147.
- <sup>18</sup>Strelets, M., "Detached Eddy Simulation of Massively Separated Flows," AIAA Paper 2001-0879, Jan. 2001.
- <sup>19</sup>Squires, K. D., Forsythe, J. R., Morton, S. A., Strang, W. Z., Wurtzler, K. E., Tomaro, R. F., Grismer, M. J., and Spalart, P. R., "Progress on Detached-Eddy Simulation of Massively Separated Flows," AIAA Paper 2002-1021, Jan. 2002.
- <sup>20</sup>Forsythe, J. R., Squires, K. D., Wurtzler, K. E., and Spalart, P. R., "Detached-Eddy Simulation of Fighter Aircraft at High Alpha," *Journal of Aircraft*, Vol. 41, No. 2, 2004, pp. 193–200.
- <sup>21</sup>Deck, S., Garnier, E., and Guillen, P., "Turbulence Modelling Applied to Space Launcher Configurations," *Journal of Turbulence*, Vol. 3, No. 57, 2002, pp. 1–21.
- <sup>22</sup>Spalart, P. R., and Allmaras, S. R., "A One Equation Turbulence Model for Aerodynamic Flows," AIAA Paper 92-0439, Jan. 1992.
- <sup>23</sup>Spalart, P. R., and Allmaras, S. R., "A One Equation Turbulence Model for Aerodynamic Flows," *La Recherche Aérospatiale*, Vol. 1, Jan. 1994, pp. 5–21.
- <sup>24</sup>Spalart, P., "Trends in Turbulence, Treatments," AIAA Paper 2000-2306, June 2000.
- <sup>25</sup>Nikitin, N. V., Nicoud, F., Wasistho, B., Squires, K. D., and Spalart, P. R., "An Approach to Wall Modeling in Large Eddy Simulation," *Physics of Fluids*, Vol. 12, July 2000, pp. 1629–1631.
- <sup>26</sup>Piomelli, U., Balaras, E., Squires, K. D., and Spalart, P. R., "Interaction of the Inner and Outer Layers in Large Eddy Simulations with Wall-Layer Models," *International Journal of Heat and Fluid Flows*, Vol. 24, 2003, pp. 538–550.
- <sup>27</sup>Deck, S., "Simulation Numérique des Charges Latérales Instationnaires sur des Configurations de Lanceur," Ph.D. Dissertation, Dept. of Fluid Mechanics, Univ. d'Orléans, Orleans, France, Oct. 2002.
- <sup>28</sup>Labourasse, E., and Sagaut, P., "Reconstruction of Turbulent Fluctuations Using a Hybrid RANS/LES Approach," *Journal of Computational Physics*, Vol. 182, No. 1, 2002, pp. 301–336.
- <sup>29</sup>Batten, P., Goldberg, U., and Chakravarthy, S., "Interfacing Statistical Turbulence Closures with Large-Eddy Simulation," *AIAA Journal*, Vol. 42, No. 3, 2004, pp. 485–492.
- <sup>30</sup>Schluter, J. U., Pitsch, H., and Moin, P., "Large-Eddy Simulation Inflow Conditions for Coupling with Reynolds-Averaged Flow Solvers," *AIAA Journal*, Vol. 42, No. 3, 2004, pp. 478–484.
- <sup>31</sup>Sagaut, P., Garnier, E., Tromeur, E., Larchevêque, L., and Labourasse, E., "Turbulent Inflow Conditions for Large-Eddy Simulation of Compressible Wall-Bounded Flows," *AIAA Journal*, Vol. 42, No. 3, 2004, pp. 469–477.
- <sup>32</sup>Breuer, M., Jovicic, N., and Mazaev, K., "Comparison of DES, RANS and LES for the Separated Flow Around a Flat Plate at High Incidence," *International Journal for Numerical Methods in Fluids*, Vol. 41, 2003, pp. 357–388.
- <sup>33</sup>Shur, M., Spalart, P. R., Strelets, M., and Travin, A., "Detached-Eddy Simulation of an Airfoil at High Angle of Attack," *4th International Symposium on Eng. Turb. Modelling and Measurements*, Elsevier, 1999.
- <sup>34</sup>Spalart, P. R., "Young-Person's Guide to Detached Eddy Simulation Grids," NASA CR-2001-211032, July 2001.
- <sup>35</sup>Aupoix, B., Guenot, D., and Sagaut, P., "ATAC: Amélioration des Modèles de Turbulence pour Prévoir l'Écoulement dans la Tuyère et sur Parrière Corps," ONERA, Rept. 64/00144 DAFE/DMAE, May 2001.
- <sup>36</sup>Travin, A., Shur, M., Strelets, M., and Spalart, P. R., "Detached-Eddy Simulations past a Circular Cylinder," *International Journal of Flow Turbulence and Combustion*, Vol. 23, 2000, pp. 293–313.
- <sup>37</sup>Molton, P., and Jacquin, L., "Étude de l'Écoulement Instationnaire Autour du Profil Transsonique OAT15A," ONERA, Rept. 187/05626 DAAP/DAFE, April 2003.
- <sup>38</sup>Jacquin, L., Molton, P., Deck, S., Maury, B., and Soulevant, D., "An Experimental Study of Shock Oscillation over a Transonic Supercritical Profile," AIAA Paper 2005-4902, June 2005.
- <sup>39</sup>Esquieu, S., "Numerical Simulation and Drag Extraction Using Patched Grid Calculations," AIAA Paper 2003-1238, Jan. 2003.
- <sup>40</sup>Sagaut, P., *Large-Eddy Simulation for Incompressible Flows*, Springer-Verlag, Berlin, 2002.
- <sup>41</sup>Deck, S., "Simulations Numériques de Type URANS-DES des Instabilités Aérodynamiques de Profil en Régime Transsonique," ONERA, Rept. 201.07381 DAAP, Oct. 2003.
- <sup>42</sup>Delcayre, F., and Dubief, Y., "On Coherent-Vortex Identification in Turbulence," *Journal of Turbulence*, Vol. 1, No. 11, 2000, pp. 1–22.
- <sup>43</sup>Deck, S., "Detached Eddy Simulation of Transonic Buffet over a Supercritical Airfoil," AIAA Paper 2004-5378, Aug. 2004.
- <sup>44</sup>Bendat, J. S., and Piersol, A. G., *Random Data: Analysis and Measurements Procedures*, Wiley-Interscience, New York, 1971.
- <sup>45</sup>Kay, S., *Modern Spectral Estimation. Theory and Application*, Prentice-Hall, Englewood Cliffs, NJ, 1987, pp. 72–77.
- <sup>46</sup>Deck, S., and Nguyen, A. T., "Unsteady Side Loads in a Thrust Optimized Contour Nozzle at Hysteresis Regime," *AIAA Journal*, Vol. 42, No. 9, 2004, pp. 1878–1888.

<sup>47</sup>Kay, S. M., and Marple, S. L. J., "Spectrum Analysis—A Modern Perspective," *Proceedings of the IEEE*, Vol. 69, No. 11, 1981, pp. 1380–1419.

<sup>48</sup>Burg, J. P., "Maximum Entropy Spectral Analysis," *Modern Spectrum Analysis*, edited by D. G. Childers, IEEE Press, New York, 1978, pp. 34–41.

<sup>49</sup>Welch, P. D., "The Use of Fast Fourier Transform for the Estimation of Power Spectra: A Method Based on Time Averaging over Short Modified Periodograms," *IEEE Trans. Audio. Electroacoustic*, Vol. AU-15, No. 2, 1967, pp. 70–73.

<sup>50</sup>Larcheveque, L., Sagaut, P., Le, T. H., and Compte, P., "Large-Eddy Simulation of a Compressible Flow in a Three-Dimensional Open Cavity at High Reynolds Number," *Journal of Fluid Mechanics*, Vol. 516, 2004, pp. 265–301.

<sup>51</sup>Rockwell, D., "Oscillations of Impinging Shear Layers," *AIAA Journal* Vol. 21, No. 5, 1983, pp. 645–664.

<sup>52</sup>Atassi, H. M., "Feedback in Separated Flows over Symmetric Airfoils," AIAA Paper 84-2297, Oct. 1984.

<sup>53</sup>Lee, B. H. K., "Transonic Buffet on a Supercritical Airfoil," *Aeronautical Journal*, May 1990, pp. 143–152.

<sup>54</sup>Girard, S., "Etude des Charges Latérales dans une Tuyère Supersonique Surdétendue," Ph.D. Dissertation, Dept. of Mechanical Engineering, Univ. de Poitiers, Poitiers, France, Dec. 1999.

<sup>55</sup>Ho, C. M., and Nosseir, N. S., "Dynamics of an Impinging Jet. Part 1. The Feedback Phenomenon," *Journal of Fluid Mechanics*, Vol. 105, 1981, pp. 119–142.

H. Reed  
Associate Editor